Dynamics and variability in regenerative potential of neuronal subtypes in the *Nematostella* nerve net

Jamie A. Havrilak[1], Layla Al-Shaer[1], Nesli Akinci[1], Aldine Amiel[2], Eric Röttinger[2], Michael J. Layden[1*]

[1] Lehigh University, Department of Biological Sciences, Bethlehem, PA

[2] Université Nice Sophia Antipolis UMR 7284, CNRS UMR 7284, INSERM U1081, Institute for Research on Cancer and Aging, Nice, France

[*] Corresponding Author: layden@lehigh.edu

Keywords: *Nematostella*, Regeneration, Neurogenesis, Nerve net, LWamide, Regenerative neurogenesis, Nervous system scalability

Abstract:

The cell dynamics and responses of individual neuronal cell types during whole-body axis regeneration are not well understood in any system. We exploited transgenic technology to track individual neuronal subtypes within regenerating *Nematostella vectensis* nerve nets *in vivo*. Individual neuronal subtypes had specific responses that included always, never, and conditional regeneration. Regenerates were smaller than the pre-amputated animal, and the nerve net was reduced in neuronal number. The reduced nerve net in regenerates led us to investigate whether the nerve net scaled with changes in body size. Neuronal number decreased as animals shrunk in response to starvation. Conversely, neurons increased in fed animals as they increased in length. The increase and decrease of neurons was reversible by switching fed animals to starvation and vice versa. Regenerates and starved/fed animals with scaled-down or scaled-up nervous systems responded to external mechanical cues. These data suggest that the *Nematostella* nerve net is dynamic, capable of scaling with changes to overall body size, and that individual neuronal subtypes display differential regenerative potential which is likely linked to the scale-state of regenerating nervous system.

Introduction:

How entire nervous systems reform in the context of whole-body axis regeneration is not well understood. Work in hydrozoan cnidarians and planarians have provided insights on some of the general molecular mechanisms that promote regenerative neurogenesis (Cebrià et al. 2002; Currie & Pearson 2013; Chen et al. 2013; Deochand et al. 2016; Gahan et al. 2017; Galliot et al. 2007; Miljkovic-Licina et al. 2007; Siebert et al. 2018; Roberts-Galbraith et al. 2016), but details about when and how individual neuronal subtypes respond are currently lacking. For example, it is currently unknown if all neuronal subtypes regenerate new neurons lost by amputation. In planarians, the total number of neurons for some neuronal fates positively correlates with the length of the animal (Takeda et al. 2009), but tracking individual neuronal fates *in vivo* in planarians is currently not feasible. As such it is not clear if neuronal number is dynamic within any one individual. The lack of understanding about the cellular dynamics during whole-body axis regeneration limits our ability to interpret functional

studies aimed at understanding the molecular mechanisms that re-pattern whole nervous systems.

The cnidarian sea anemone *Nematostella vectensis* offers the potential to track individual neuronal fates throughout the process of regeneration. *Nematostella* is an optically clear diploblastic animal. The primary axis is the oral-aboral axis. The oral pole possesses a single mouth surrounded by up to 16 tentacles (Fritz et al. 2013). Eight segments radially situated around the mouth run the length of the oral-aboral axis. Each radial segment contains a mesentery, which contains gonads, a number of differentiated cells, longitudinal tracts of neurites, and longitudinal myoepithelial cells (Tucker et al. 2011; Renfer et al. 2010; Jahnel et al. 2014; Steinmetz et al. 2017; Williams 1975). The *Nematostella* nervous system is a typical cnidarian nerve net, which initially forms during embryonic and larval stages in both the ectoderm and endoderm (Rentzsch et al. 2016; Nakanishi et al. 2012). A number of transgenic lines exist, which allows for *in vivo* tracking of individual cell types (Layden et al. 2016; Nakanishi et al. 2012; Richards & Rentzsch 2014; Renfer et al. 2010; Havrilak et al. 2017; Busengdal & Rentzsch 2017). Using *in vivo* characterization of the *NvLWamide-like::mCherry* transgene, we identified at least five neuronal subtypes, determined that some of those neuronal subtypes form in a highly stereotyped manner, and that the number of some neuronal subtypes correlates with length (Layden et al. 2016; Havrilak et al. 2017).

Here, we exploited the ability to track individual neuronal subtypes using *NvLWamide-like::mCherry* transgenic animals during whole-body axis regeneration and during feeding and starvation treatments. *Nematostella* regenerates were smaller than their parent uncut animal, and their nervous systems had reduced numbers of at least some neuronal subtypes. Neurons were classified into at least three classes based on their specific regenerative responses: Class I neurons, which regenerated under all circumstances; Class II neurons, which did not appear to regenerate; and Class III neurons, which displayed differential regenerative potential that appeared to depend on the size of the remnant fragment. The reduced size of the regenerated nervous system led us to investigate scalability of the nerve net. Fed or starved *Nematostella* grew or shrunk respectively, and the nervous system responded in part by modifying the number of some neuronal subtypes to scale with changing polyp length. Despite their reduced nervous

systems, regenerates and animals that had been starved still responded to being touched and were capable of feeding, suggesting that the reduction does not inhibit functionality. These data suggest that the *Nematostella* nerve net is highly dynamic and scales with body size. To the best of our knowledge, these findings are the first evidence that regenerative responses of individual neurons are variable during whole-body axis regeneration. These data indicate that the molecular mechanisms enacted to promote regenerative neurogenesis likely vary based on the size of the remnant fragment and which neuronal subtypes must regenerate.

Results:

Neuronal subtypes display differential regenerative potentials.

To determine how neuronal subtypes regenerate, our goal was to bisect animals into two equal halves (*Oral* and *Aboral* remnants) and measure the neuronal response in *Aboral* remnants (Figure 1A). We focused on *Aboral* remnants because there are morphological indicators for when regeneration has completed and a well-established regenerative time course (Passamaneck & Martindale 2012; Amiel et al. 2015; Bossert et al. 2013). One challenge was that animals do not always relax completely or uniformly along the oral-aboral axis when treated with $MgCl_2$, and the wound site on both remnants curls in, which makes using measurements to ensure the cut site is always in the same position unreliable. However, the number of longitudinal neurons in the *NvLWamide-like::mCherry* transgenic animals scale with animal length and appear to be evenly distributed along the oral-aboral axis (Havrilak et al. 2017). We reasoned that if evenly distributed, quantifying longitudinal neurons pre- and post-amputation could be used as a proxy for length, and allow us to confirm amputation occurred in the intended location. The oral-aboral axis was divided into 4 equal quarters, and the longitudinal neurons were quantified in each quarter in animals of various lengths. Each quarter contained similar numbers of longitudinal neurons with no statistical difference between the numbers of neurons in any of the quarters (Figure 1B). Thus, we were justified in using longitudinal number to track amputation sites and as a proxy for length.

To quantify regeneration of individual neuronal subtypes we used animals that were 2.5 to 8.5 mm long (Supplemental Figure 1A), because this range represents the

125 sizes of naturally occurring wild-caught animals found along the East Coast of the United
126 States (Adam Reitzel, personal communication, 11/2018). Animals in this size range also
127 have a manageable number of longitudinal and tripolar neurons for quantification. We
128 focused on longitudinal, tripolar, pharyngeal, and tentacular neuron subtypes described
129 by the *NvLWamide-like::mCherry* transgene (Havrilak et al. 2017). Tentacular and
130 pharyngeal neurons are specifically located at the oral end of the animal, whereas
131 longitudinal and tripolar are evenly distributed along the oral-aboral axis in the endoderm
132 and ectoderm, respectively (Figure 1C) (Havrilak et al. 2017; Layden et al. 2016). We
133 excluded the *NvLWamide-like::mCherry*+ mesentery neurons from this analysis. This is
134 because the ruffled mesentery structure and large number of mesentery neurons made
135 quantification unreliable. With the *NvLWamide-like::mCherry* line it is possible to easily
136 score for the regeneration of oral specific neurons (tentacular and pharyngeal), as well as
137 track regeneration of an individual neuronal subtype in both the endoderm and ectoderm.
138 To characterize neuronal subtype regeneration animals were allowed to relax,
139 $MgCl_2$ was added to relaxed animals, and the number of longitudinal and tripolar neurons
140 were quantified (*uncut*) (Figure 1C, F, and H). Animals were then bisected in half and
141 longitudinal and tripolar neurons were quantified in the *Aboral* remnant (*time 0 cut*)
142 (Figure 1D, F-I; Supplemental Figure 2). This process takes less than 20 minutes/animal.
143 $MgCl_2$ was then washed out and animals were allowed to regenerate in 1/3x artificial sea
144 water, (hereafter called *Nematostella* medium). Because extensive cell death occurs over
145 the first 24 hours of regeneration (Warner et al. 2019), regenerating *Aboral* remnants
146 were paralyzed using $MgCl_2$ and neuronal number was reassessed again at 24 hours post
147 amputation (*24hpa*) (Figure 1F-I; Supplemental Figure 2). $MgCl_2$ was again washed out
148 and animals were allowed to regenerate until 7 days post amputation (dpa) when neuronal
149 numbers were quantified a final time (*7dpa*) (Figure 1E, F-I; Supplemental Figure 2). All
150 oral structures including mouth, pharynx and tentacles regenerated in the aboral remnant
151 by *7dpa* (Figure 1E; Supplemental Figure 3), which is consistent with previous findings
152 and suggests that $MgCl_2$ treatments did not impact regenerative timing (Amiel et al. 2015;
153 Passamaneck & Martindale 2012). Regenerates were reduced in size compared to pre-
154 amputated animals, as indicated by a reduction in overall length (Figure 1 C and E;
155 Supplemental Figure 1A-C) and decreased longitudinal and tripolar neuronal numbers

156 (Figure 1F-I; Supplemental Figure 2). On average regenerates from animals bisected at
157 the midpoint were ~65% of their pre-amputated length at *7dpa*, with the caveat that
158 precise length measurements were difficult (Supplemental Figure 1A and B).
159 Nevertheless, it is clear that regenerates did not return to their precut length, and that
160 longitudinal and tripolar neurons were decreased compared to the uncut starting number
161 for all regenerates. We conclude that the nerve net of regenerates is reduced in terms of
162 neuronal number compared to the uncut parental animal.

163 We observed pharyngeal and tentacular neuron regeneration in 100% of 7dpa
164 regenerates (N = 73; Figure 1E; Supplemental Figure 3). Further characterization
165 suggested that tentacular neurons were visible in the forming tentacle buds by 72hpa, and
166 that pharyngeal neurons were first detected between 48 and 72hpa (Supplementary Figure
167 3). We concluded that both tentacular and pharyngeal neurons regenerated and their
168 regeneration coincides with the re-appearance of their corresponding tissues.

169 To better understand regeneration of longitudinal and tripolar neurons, which are
170 present in both the *Aboral* remnant and regenerates, we quantified changes in neuronal
171 number throughout regeneration (Figures 1F-I). Since the number of longitudinal neurons
172 never returned to the initial starting numbers in any of the animals, we focused our
173 investigation on the time between when they were cut (*time 0 cut*) and after they fully
174 regenerated (*7dpa*) (Figures 1 G and I, boxed regions in F and H, respectively).

175 We initially treated all regenerates equal regardless of size, but observed
176 differential regeneration of longitudinal neuronal subtypes that appeared to be size
177 dependent. For the remainder of analysis we will describe the longitudinal and tripolar
178 regeneration in four different size groups, based on the starting number of longitudinal
179 neurons present in the uncut animal. We categorized animals as small (20-40 longitudinal
180 neurons or ~2.5-5 mm), medium (41-60 longitudinal neurons or ~3.5-5.5 mm), medium-
181 large (61-80 longitudinal neurons or ~5-7.5mm), and large (81-100 longitudinal neurons
182 or ~6.5-8.5 mm) (Supplemental Figure 1A). Both size and longitudinal number were used
183 to classify animals for the reasons discussed above.

184 Longitudinal neurons regenerated in small and medium animals, but not medium-
185 large or large animals. Between *time 0 cut* and *24hpa* the number of longitudinal neurons
186 initially decreased in all size groups (Figure 1G, all $p < 0.001$), likely due to increased

187 apoptosis that occurs over the first 24hpa (Warner et al. 2019). The number of
188 longitudinal neurons significantly increased between *24hpa* to *7dpa* in small and medium
189 animals ($p < 0.001$ and $p = 0.001$, respectively). The numbers of longitudinal neurons in
190 *7dpa* regenerates were statistically similar to the numbers observed in *time 0 cut* animals
191 for both small and medium groups (small: $p = 0.77$, medium: $p = 1.00$), suggesting
192 longitudinal neurons regenerated back to their numbers present in the remnant fragment
193 at the time of bisection (Figure 1G, red and green lines). No regeneration of longitudinal
194 neurons was observed in medium-large and large animals between *24hpa* and *7dpa*
195 (Figure 1G, yellow and blue lines; $p = 0.249$ and $p = 1.00$, respectively). Despite the
196 differences in regenerative potentials of the longitudinal neurons, there was no significant
197 difference in the percent length of regenerates at *7dpa* relative to their starting size
198 (Supplemental Figure 1B).
199 In contrast to longitudinal neurons, there was no regeneration of tripolar neurons
200 in any of the animal size groups. The number of tripolar neurons decreased between *time*
201 *0 cut* and *24hpa* (Figure 1I, $p < 0.001$) but failed to return to the *time 0 cut* numbers by
202 *7dpa* (Figure 1I, $p < 0.001$).
203 We conclude that longitudinal neurons display differential regenerative potential
204 that corresponds to the size of the pre-amputated animal, and that tripolar neurons do not
205 demonstrate any regenerative potential.
206
207 **Differential regenerative potential of longitudinal neurons depends on the size of the**
208 **remnant fragment.**
209 We wondered what was influencing the variable regenerative potential of
210 longitudinal neurons. All animals, including our large group animals (Supplemental
211 Figure 4), show increased proliferation in both the ectoderm and endoderm of
212 regenerating tissue. This observation is consistent with the finding that *Nematostella*
213 regeneration has been described to be dependent on cell proliferation (Amiel et al. 2015;
214 Passamaneck & Martindale 2012). Two obvious factors that might influence the
215 regenerative potential of longitudinal neurons are the animal's pre-amputation size or the
216 size of the *Aboral* remnant. If the remnant size plays a role in regenerative potential, then
217 shifting the amputation site in large and small animals to create larger or smaller remnant

218 fragments should alter the regenerative potential of longitudinal neurons. However, if the
219 animal's pre-amputation size dictates regenerative potential, then altering the amputation
220 site should not alter regenerative potential of longitudinal neurons.
221 When smaller *Aboral* fragments were generated from large animals by aborally
222 shifting the amputation site to remove 75% of the oral-aboral axis (Figure 2A),
223 longitudinal neurons regenerated between *24hpa* and *7dpa* (Figure 2C, $p = 0.046$).
224 Interestingly, the remnant fragment generated by the aboral shift resulted in a similar
225 number of longitudinal neurons at *time 0 cut* and *24hpa* as the fragment from medium
226 animals bisected into equal halves (Figure 2D, compare black and faded green lines).
227 Alternatively, orally shifting the amputation site of medium sized animals to remove only
228 25% of the oral-aboral axis (Figure 2B) increased the remaining number of remaining
229 longitudinal neurons at *24hpa* similar to those remaining in medium-large and large
230 animals bisected into two equal halves (Figure 2 E and F, compare black and faded blue
231 and yellow lines), and similarly resulted in no longitudinal neuron regeneration between
232 *24hpa* and *7dpa* ($p = 1.00$). When the amputation site of small animals is orally shifted
233 (Figure 2B), the increased *Aboral* remnant fragment has a similar number of remaining
234 longitudinal neurons as the fragment generated by bisecting a medium animal into two
235 equal halves (Figure 2G and H, black lines). Longitudinal neurons showed a trend
236 towards regeneration in small animals with an orally shifted amputation site, similar to
237 the medium sized animals (Figure 2G, H, compare black and faded green lines) but the
238 increase in number between *24hpa* and *7dpa* was not statistically significant ($p = 0.469$)
239 However, the number of neurons at *7dpa* is also not statistically significant from the
240 number at *time 0 cut*, ($p = 0.119$), but the *time 0 cut* and *24hpa* values are different ($p <$
241 0.001), suggesting that the trend towards regeneration is real and that variability in
242 responses of small animals by *7dpa* are the source for lack of statistical significance.
243 The size of the remnant fragment appears to play a larger role in dictating the
244 regenerative potential of longitudinal neurons than the starting size of the pre-amputated
245 animal. Overall, these data suggest there are at least three regenerative responses for
246 neuronal subtypes in *Nematostella.* Class I neurons that regenerate 100% of the time
247 following amputation (tentacular and pharyngeal *NvLWamide-like* neurons); Class II
248 neurons, which do not regenerate by *7dpa* (tripolar *NvLWamide-like* neurons); and Class

249 III neurons that have differential regenerative abilities likely controlled in part by the size
250 of the remnant fragment (longitudinal *NvLWamide-like* neurons).
251
252 **Longitudinal and tripolar neuron numbers are dynamic and scale with size in adult**
253 **animals.**
254 The reduced size of the regenerated nerve net following amputation led us to
255 investigate scalability. The number of longitudinal and tripolar neurons positively
256 correlate with animal length during growth from juvenile polyps into adult stages
257 (Havrilak et al. 2017). Because regenerates are smaller than pre-amputated animals, and
258 the number of longitudinal and tripolar neurons are reduced in regenerates (Figures 1 and
259 2; Supplemental Figure 2), we wondered if longitudinal and tripolar numbers might
260 fluctuate in adult animals as they grow and shrink in size. *Nematostella* increase in size
261 when fed (Figure 3 A, B, and G)(Hand & Uhlinger 1992; Layden et al. 2016), and our
262 observations demonstrate that they decrease in size when starved (Figure 3A, B, and G).
263 Thus, we set out to determine if tripolar and longitudinal neuronal numbers are dynamic
264 in adults that are increasing and decreasing in size.
265 To compare responses, we performed two replicate experiments that varied the
266 number of starting longitudinal and tripolar neurons and therefore the starting size of the
267 animals (Figure 3, smaller animals; Supplemental Figure 5, larger animals). The initial
268 experimental design was to track neuronal number in animals over fourteen weeks.
269 Animals would be either starved or fed for seven weeks, then the feeding regimen would
270 be changed for the remaining seven weeks. However, we found our largest animals that
271 were initially fed (the feed-starve treatment group) became too large to accurately count
272 within the time constraints of our paralytic after 3 weeks into our feeding regimen. We
273 therefore switched the animals to starvation for the remaining 11 weeks in both
274 independent experiments (Figure 3; Supplemental Figure; black lines).
275 After the initial 3 weeks of feeding, the fed then starved animals (Figure 3 and
276 Supplemental Figure 5, black lines) had significantly increased in length (Figure 3A and
277 G, $p = 0.008$), and the number of both longitudinal neurons (Figure 3C and D;
278 Supplemental Figure 5A and B; $p < 0.001$ for both) and tripolar neurons (Figure 3E and
279 F, $p = 0.32$; Supplemental Figure 5C and D, $p < 0.001$) significantly increased. Following

280 the switch to a starvation regime, the fed then starved animals significantly shrunk in size
281 after 11 weeks (Figure 3A and G, $p = 0.008$), and lost a significant number of
282 longitudinal (Figure 3C and D, $p = 0.003$; Supplemental Figure 5A and B, $p = 0.001$) and
283 tripolar neurons (Figure 3E and F, $p = 0.031$; Supplemental Figure 5C and D, $p < 0.001$).
284 Animals placed on the opposite feeding regime had opposite effects on their size
285 and neuronal number (Figure 3B-G; Supplemental Figure 5A-D, blue lines). The animals
286 that were initially starved for 7 weeks (starved then fed group) got smaller in size (Figure
287 3B) and their measured length showed a trend toward a shorter length (Figure 3G, $p =$
288 0.098), suggesting the animal is slower to shrink in size than grow. Starved then fed
289 animals showed significant decreases in longitudinal neurons during the starvation
290 regime (Figure 3C and D, $p = 0.004$; Supplemental Figure 5A and B; $p = 0.031$). Tripolar
291 neurons significantly decreased in the animals that were initially smaller to start (Figure
292 3E and F, $p = 0.029$), and their decrease approached significance in animals that were
293 larger to start (Supplemental Figure 5 C and D, $p = 0.094$). When switched to feeding, the
294 starved then fed animals significantly increased in size (Figure 3B, 3G, $p < 0.001$) and
295 both neuronal subtypes significantly increased in number (Figure 3C-F, Supplemental
296 Figure 5 A-D; $p \leq 0.001$ for all).
297 We conclude that *Nematostella* scales at least part of its nervous system by
298 altering neuronal subtype number coincidently with increases or decreases in its size.
299
300 **Increased Caspase 3 activity in neuron-like cells is observed in starved animals**
301 Increase in neuronal number is due to birth of new neurons, and increased
302 apoptosis is the most likely cause for decrease in neuronal number. To assess if the loss
303 of neurons in starved animals is correlated with increased apoptosis, we stained fed and
304 starved animals with an α–Caspase 3 antibody that recognizes the p17 fragment of active
305 Caspase-3, a potential marker of apoptosis. Caspase-3 is an effector of the apoptosis
306 pathway (Elmore 2016) and has been identified as a key mediator in neuronal
307 programmed cell death (D'Amelio et al. 2012; Kuida et al. 1996). The *Nematostella*
308 genome possesses at least three *caspase 3* orthologs (Moya et al. 2016). Using the active
309 Caspase-3 antibody on fed *versus* 3-week starved animals, we observed activated
310 Caspase 3 staining in 15 out of 15 of starved animals (Figure 4), which is in contrast to

311 the Caspase-3 staining only being observed in 2 of the 16 fed animals. Activated
312 Caspase-3 was detected in cells located along the longitudinal tracts of starved animals
313 (Figure 4E-H, arrow), as well as in cells throughout the body column of starved animals
314 (Figure 4E-H, arrowhead). Interestingly, some of the activated Caspase3 positive cells
315 had a neuronal-like morphology, suggesting that neuronal death does occur during
316 periods of starvation.
317 Our data suggest that apoptosis is not only playing a role in the loss of cells,
318 including some neuron populations in the starved animals, but also that apoptosis is
319 restricted primarily to the physa, which is the most aboral region of the body. We
320 conclude that starvation induces an increase in Caspase 3 activity in neuronal and non-
321 neuronal cells, which suggests that decreases in animal size are due to induced cell death.
322
323 **Scaled down nervous systems maintain the ability to respond to external cues**
324 Lastly, we wondered if the *Nematostella* nervous system retained function in each
325 scale state. However, *Nematostella* are known to retract when challenged with a
326 mechanical stimulus. Thus, we decided to determine if *Nematostella* retained the ability
327 to respond to mechanical cues in different scale states. Because there are no quantified
328 behavioral assays available yet in *Nematostella*, we developed an action-reaction Poking
329 assay using a toothpick to induce a reaction response. Poking an animal near the tentacles
330 induced a contraction of the animal away from the stimulus (see Supplemental Movies 1-
331 6). Each animal was poked three times in the most oral region of the body, and a positive
332 response was scored when the animal retracted their tentacles and/or their body at least
333 once in response to being poked. We observed variable responses to the Poking assay
334 (anywhere from entire body retraction to only retracting 1-2 tentacles). Therefore any
335 attempt to move their body away from the toothpick was classified as a positive response.
336 We first examined the behavioral response in pre- and post- regenerated animals
337 (Figure 5; Table 1). For all the cases (N = 8), the same animal responded to the Poking
338 assay both pre-bisection (Figure 5A-D) and *7dpa* (Figure 5E-H; Table 1). After
339 regeneration, the nerve net and the number of neurons it contained were decreased
340 compared to the initial non-bisected body (Figures 1 and 2; Supplemental Figure 2). The
341 maintenance of the behavioral response in the regenerated animal suggests that the

342 reduction in the nervous system size did not limit the animal's ability to coordinate a
343 response to external mechanical cues.
344 We next performed the Poking assay in fed *versus* starved animals (Figure 6;
345 Table1). We observed that animals starved (6-7 weeks) or fed (3 weeks) both responded
346 to the Poking assay (Figure 6A-E, H-M; Table 1). As expected, we observed a significant
347 decrease of the numbers of longitudinal and tripolar neurons in the starved animals
348 (Figures 6F and G) and a significant increase in these neuronal numbers in the fed
349 animals (Figure 6N and O). We conclude that retraction in response to a mechanical cue
350 behavior is not dependent on the size of the nervous system. These preliminary findings
351 suggest that the neurocircuitry for at least some behaviors are retained regardless of the
352 overall size of the nerve net.
353
354 **Discussion:**
355
356 **Variability in regenerative potential of individual cell types during whole-body axis**
357 **regeneration.**
358 This study represents the first study we are aware of to track neuronal subtype
359 regeneration *in vivo* in individuals undergoing whole-body axis regeneration. We found
360 that individual neuronal subtypes have differential potential to regenerate new neurons,
361 and this is based in part on the size of the remnant fragment. We therefore grouped
362 neurons into three classes based on regenerative response. Class I neurons that
363 regenerated 100% of the time, Class II neurons that did not regenerate following
364 amputation, and Class III neurons, which are perhaps the most interesting, because they
365 are capable of regenerating under some but not all circumstances. We were initially
366 concerned that the lack of regeneration observed in Class II and sometimes Class III
367 neurons was due to delayed regeneration, particularly in larger animals. Regeneration
368 occurred within seven days regardless of the size of the animal. Larger animals would
369 need to regrow more tissue to go from ~50% (following amputation) to ~65% pre-cut
370 length (after regeneration) (Supplemental Figure 1). To accomplish this, they would need
371 to proliferate more rapidly than smaller animals and an increase in proliferation rates
372 could delay longitudinal differentiation, whereas tripolar regeneration could be delayed in

373 all cases. We did check regenerates at 12 and 14dpa and we saw no change from the
374 neuronal numbers observed at 7dpa (data not shown), suggesting that there is no delay in
375 longitudinal specification in larger animals nor any delay in tripolar regeneration. We
376 argue that there is fundamental difference in why longitudinal neurons regenerate in
377 smaller but not larger remnant fragments, and that Class II and Class III neurons are both
378 part of the normal regenerative response.
379 It is likely that all three neuronal classes described here are present in other
380 animals. Class I neurons were neurons that were present in structures that needed to
381 completely reform in regenerates. Within planarian whole-body axis regeneration, Class I
382 neurons would likely be any of the neuronal subtypes present specifically in the brain or
383 eyes that needed to regenerate following amputation of anterior regions. It is not clear
384 how widespread the presence of Class II neurons is in animals, because tracking of
385 individual neuronal subtypes during regeneration in the same animal has not been
386 reported in planarians or *Hydra*. Given that both planarians and *Nematostella* have been
387 shown to have nervous systems that scale with size (Figures 3; Supplemental Figure 5)
388 (Takeda et al. 2009), it is likely that Class II neurons are not a *Nematostella* specific
389 phenomenon. It should be noted that Class II neurons are capable of regenerating in some
390 regenerative paradigms. Tripolar neurons that were lost as animals shrunk during
391 starvation repopulated in animals that regrew once they were switched back to feeding
392 (Figure 3 and Supplemental Figure 5). This suggests that the regenerative potential of any
393 neuronal subtype is not uniform across all regeneration paradigms. There is evidence for
394 Class III-like regenerative potential in other animals. For example, populations of
395 dopaminergic neurons in the brains of adult zebrafish have been shown to be diverse in
396 their regenerative capacity (Caldwell et al. 2019). Based on the fact that regenerates are
397 smaller than the pre-cut animal, that degrees of nervous system scaling is likely common
398 in animals, and that some amputations result in complete loss of some neuronal subtypes,
399 we predict that all three neuronal classes are common to all animals that undergo whole-
400 body axis regeneration.
401
402 ***Nematostella* nervous system scales with animal length.**

403 *Nematostella* modulated the size of its nerve net by increasing or decreasing
404 neuronal number in response to feeding or starvation periods, and these changes were
405 reversible (Figure 3). The correlation between neuronal number and body size suggests
406 that *Nematostella* scales its nervous system with its body size. Importantly, *Nematostella*
407 maintains normal behaviors in each scale state (Figures 5 and 6). The potential scalability
408 of nervous systems has been suggested by studies using molecular markers to track
409 neuronal subtypes in planarians. Specific cell types, including visual cells and neural cells
410 in the brain, were shown to correlate with body length, and there is also a constant ratio
411 maintained between several types of neurons in the brain regardless of overall number
412 (Takeda et al. 2009). Although this planarian study was performed in fixed animals, their
413 findings are consistent with the dynamic and scalable nervous system found in
414 *Nematostella.* It should be noted that we did not address, and do not we rule out, that the
415 *Nematostella* nervous system may also scale by modulating connectivity of existing
416 neurons.
417 During both regeneration and body scaling, *Nematostella* retains normal body
418 form (Figures 1 and 3), the ability to respond to a mechanical cue (Figures 5, 6), and the
419 ability to eat (Passamaneck & Martindale 2012; Layden et al. 2016). Additionally, even
420 with a smaller nerve net, we can infer that these animals are telling the difference
421 between a potential predator (toothpick) and prey (brine shrimp), because while the
422 animals responded to the Poking assay with a defensive retraction, they readily capture
423 and ingest the food. Taken together these observations suggest that the nervous system is
424 functional in all scale states.
425
426 **Nervous system scalability may influence regenerative potential of neuronal**
427 **subtypes.**
428 The fact that nervous systems scale with size in *Nematostella,* and that
429 regenerates are smaller than pre-cut animals, suggests that the differential regenerative
430 responses of individual neurons are linked to the scale state of the regenerate. The two
431 neuronal subtypes that we confirmed have reduced numbers in regenerates are the
432 longitudinal (Class III) and tripolar neurons (Class II). Coincidently, the total number of
433 neurons for both of these neuronal subtypes correlate with overall length and scale in

434 number as animal length increases or decreases (Figure 3; Supplemental Figure
435 5)(Havrilak et al. 2017). While it is logical that regenerates that are smaller than the pre-
436 cut animal have less tripolar and longitudinal neurons, it is not clear why tripolar neurons
437 do not show regenerative potential, but longitudinal neurons do under some
438 circumstances. One possible explanation for why tripolar neurons do not regenerate is
439 that the number of neurons present in the *Aboral* remnant are within an acceptable range
440 for the scale state of the regenerate. As a result, tripolar neurons do not need to increase
441 in numbers as part of a regenerative response. An alternative explanation is that
442 regeneration of tripolar neurons may not be necessary because they may function
443 similarly to tentacular neurons. Tripolar and tentacular neurons are both ectodermal
444 neurons that share a similar morphology (Havrilak et al. 2017). The reduced size of
445 regenerates suggests that the majority of regenerated tissue is contributing to pharyngeal
446 and tentacular structures. If tentacular neurons have a similar function to the tripolar
447 neurons they may compensate until the regenerate starts to feed and tripolar neurons
448 begin populating the body column with growth. However, it should be noted that tripolar
449 and tentacular neurons are specified at different times during development (Havrilak et
450 al. 2017), and the tissues they arise from have distinct gene expression profiles of
451 transcription factors known to pattern neuronal fates in *Nematostella* and traditional
452 model systems (Layden et al. 2010; Sinigaglia et al. 2013; Leclère et al. 2016; Marlow et
453 al. 2013; Röttinger et al. 2012). Thus, it isn't clear if they are similar neurons that are
454 patterned using variable molecular programs during development, or if they are distinct
455 neuronal fates.
456 The differential response of longitudinal neuron regeneration observed in
457 different sized remnant fragments is interesting. We have thought of two hypotheses to
458 explain the response. The first hypothesis is simply that the scale state of longitudinal
459 neurons is different than that of tripolar neurons, and that in smaller remnants the number
460 of longitudinal neurons is below a minimum threshold, which results in induction of
461 regenerative response after amputation. In larger fragments, the number of longitudinal
462 neurons is above the minimum threshold for the new scale state of the nervous system,
463 and thus no regenerative response is induced. The alternative hypothesis is that there are
464 differences in regenerative mechanisms between large and smaller animals. Although cell

465 proliferation is required for *Nematostella* oral regeneration (Passamaneck & Martindale
466 2012), some remodeling of remnant tissue occurs (Amiel et al. 2015). These findings
467 suggest *Nematostella* uses a hybrid of cell proliferation and morphallaxis to regenerate.
468 EdU labeling suggests that larger animals are still regenerating using both cell
469 proliferation and morphallaxis, but perhaps they shift mechanisms to favor morphallaxis
470 and smaller animals favor cell proliferation. Future experiments to help distinguish
471 between potential different mechanisms of regeneration based on animal size should be
472 done to better understand *Nematostella* regeneration. Our limited studies favor the
473 threshold scale model. First, we did not observe additional longitudinal neurons in
474 regenerates from large animals bisected in half at 14dpa. Even if large animals do rely
475 more heavily on morphallaxis, they are still increasing in size at equal proportions to
476 small animals. Thus, the prediction is that longitudinal neurons should increase in number
477 unless there is a sufficient number of neurons to be at the "low" end of the acceptable
478 scale state in the regenerate. Additionally, when cut sites were shifted the regenerative
479 response of the remnant tissue was dictated by its size. This suggests that there are
480 particular scale states that need to be maintained in different sized animals. Regardless of
481 the exact mechanism, the data support the hypothesis that once we identify the key ratio
482 of neuronal number to length for a particular neuronal subtype, it should be possible to
483 predict its regenerative response based on the size and number of neurons present in the
484 remnant fragment.
485
486 **Scalability of adult *Nematostella* nerve net**
487 *Nematostella* must have a mechanism to sense and regulate the ratio of neuronal
488 number to body size. Possible mechanisms include the nervous system self-regulating
489 subtype numbers autonomously, or that neural numbers are influences by signaling from
490 neural and other tissues/cell types within the body. It is unlikely that changes in size also
491 influence the amount of other cell types besides neurons. Non-neuronal cells had
492 detectable activated Caspase-3 (Figure 4), which suggests other cell types decrease as the
493 animal length decreases during starvation. This is similar to observations in planarians
494 where an overall increase or decrease in cell number across multiple cell types
495 corresponds to larger or smaller length, respectively (Baguna et al. 1981; Romero &

496 BAGUÑÀ 1991; Takeda et al. 2009; Oviedo et al. 2003). The global change of other
497 neuronal cell types suggests that signaling between cell types may coordinate scaling of
498 the entire animal simultaneously. One example of regulation of cell number being
499 mediated by signaling between different cell types is the regulation of hematopoietic stem
500 cell number by Notch and BMP signaling from osteoblasts (Zhang et al. 2003; Bowers et
501 al. 2015; Calvi et al. 2003). However, microglia have been shown to self-regulate their
502 numbers during periods of resolution following neurodegeneration in both zebrafish (van
503 Ham et al. 2014) and mice (Tay et al. 2017). This occurs via cell egress and apoptosis
504 (Tay, 2017), and phagocytosis of disease state microglia undergoing apoptosis by other
505 viable/healthy microglia has also been demonstrated (van Ham, 2014). At this point it is
506 unclear if scaling of the nervous system occurs autonomously, is directed by signaling
507 from other tissues, or via both mechanisms. Future work characterizing *Nematostella*
508 growth and shrinking and the scaling responses of differentiated cell types is an exciting
509 potential area of research.
510
511 **Conclusion:**
512 The ability to observe and quantify individual neuronal subtypes makes
513 *Nematostella* a powerful model to investigate neurogenesis in the context of both
514 regeneration and whole-body scaling. Our data suggest that the regenerative responses of
515 neuronal subtypes in *Nematostella* are variable and depend both on individual subtypes
516 and the size of the remnant fragment. These data imply that there is differential
517 deployment of the molecular pathways that specify specific subtypes that may be
518 dependent on the scale-state of the nervous system in the regenerate. How *Nematostella*
519 controls the generation and incorporation of new neurons into the existing nerve net, and
520 how they scale the numbers of these neurons to body size in real time remains an
521 unknown, but both are exciting areas for future investigation. Lastly, our data suggest that
522 experiments aimed at uncovering the molecular mechanisms regulating neural
523 regeneration in *Nematostella* require careful consideration of the differential regenerative
524 potential of individual neuronal subtypes when designing experiments and interpreting
525 results.
526

527 **Methods:**

528

529 **Animal care**

530 All animals were kept at room temperature and fed rotifers or crushed brine
531 shrimp until they reached the young juvenile adult stage, at which time they were
532 transferred to 17 ^{o}C and switched to solely brine shrimp. All juvenile adult and adult
533 animals were housed at 17°C in the dark and fed brine shrimp 4x/week, unless otherwise
534 noted for experimental purposes. *Nematostella* were maintained in 1/3x artificial sea
535 water, (*Nematostella* medium) at a pH of 8.1-8.2 that was changed once per week.

536 *Nematostella* were relaxed in 7.14% (wt/vol) $MgCl_2$ in *Nematostella* medium for
537 ~10 minutes prior to quantification, imaging, or bisection. The lengths of relaxed animals
538 were measured in mm with a ruler placed under a Petri dish containing the animal.

539

540 **Quantification of NvLWamide-like::mCherry-expressing neurons**

541 *NvLWamide-like::mCherry* tripolar and longitudinal neurons were counted on live
542 animals under a dissection microscope (Nikon SMZ1270), on live animals placed under a
543 slide with a raised coverslip on a compound microscope (Nikon NTi), or on full-length
544 images of *Nematostella*. All quantifications of longitudinal and tripolar neurons were
545 obtained by counting the neurons from 2-4 segments on each individual animal that were
546 then averaged together.

547

548 **Regeneration experiments**

549 Longitudinal and tripolar neurons were quantified first on the uncut animal, then
550 immediately following bisection (time 0 cut), 24 hours post amputation (hpa), and 7 days
551 post amputation (dpa). Animals were either bisected in half with the cut site at oral-aboral
552 midpoint (~50% body removed), bisected below the pharynx ("oral shift", ~25%
553 removed), or bisected at the aboral end ("aboral shift", ~75% removed). Following
554 quantification and/or bisection, the remnant aboral fragment was washed with
555 *Nematostella* medium, then placed in the dark at room temperature. Prior to
556 quantification, animals were starved 4 days (Amiel et al. 2015; Passamaneck &
557 Martindale 2012). Animals were not fed for the duration of the experiment.

558

559 **Feed/Starve experiments**

560 For each animal, the number of longitudinal and tripolar neurons were counted at
561 Time 0, at the time of their feeding regime switch (starved to fed, 6-7 weeks later; fed
562 then starved 3 weeks later), and at the end of the 14 week experiment. All animals were
563 maintained on the same normal feeding schedule until Time 0 of the experiment. At this
564 time animals were randomly assigned to either the starve-feed group or feed-starve
565 group, then they were imaged, and their initial starting neural counts were taken. Animals
566 on the feeding regime were fed brine shrimp 2x/week plus oyster 1x/week, and were
567 given weekly water changes.

568

569 **Poking assay**

570 Animals were transferred to a depression slide containing *Nematostella* medium.
571 Once the animal had relaxed its tentacles a toothpick was slowly inserted into the
572 medium so as to not disturb the animal prematurely. The animal was then "poked" with
573 the tip of the toothpick at the oral region. The entire assay was video recorded and
574 analyzed to determine the animal's response. Following the "Poking assay", the animal
575 was left alone in the dish until it relaxed again, upon which the Poking assay was
576 performed again. The assay was performed 3 consecutive times. A positive response was
577 determined if the animal responded to being touched with a toothpick by retracting some
578 or all of its tentacles, scrunching or retracting in its mouth (oral region) or retracting its
579 entire body. To be considered responsive the animal had to react in at least 1 out of the 3
580 poking assays performed.

581

582 **EdU Stain**

583 EdU incorporation was carried out as previously described with modifications
584 (Fritz et al. 2013). Animals were incubated with 330uM EdU in *Nematostella* medium for
585 30 minutes, then fixed as previously described (Fritz et al. 2013) and dehydrated to 100%
586 MeOH and stored at -20 ^{o}C. Following rehydration, samples were permeabilized in PBT
587 (PBS with 0.5% Triton X-100, Sigma) for ~2 hours. Animals were then treated with the
588 reaction cocktail (prepared following the Click-It protocol provided by the manufacturer,

589 with the exception of doubling the amount of Alexa Fluor azide) at room temperature in
590 the dark for 20 minutes. Following 5 long washes in PBT the animals were labeled with
591 propidium iodide for 1 hour while rocking, washed 5X in PBT and finally transferred to
592 90% glycerol for imaging.
593
594 **Immunohistochemistry for activated Caspase-3**
595 Preparation for staining was carried out as previously described (Amiel et al.
596 2015). To analyze for activated Caspase-3 (apoptosis stain), we used a polyclonal rabbit
597 active Caspase-3 antibody (ABCAM, ab2302). Secondary Alexa Fluor 488 donkey anti-
598 rabbit (Life Technologies, A21206) was used.
599
600 **Imaging**
601 Live images of *NvLWamide-like::mCherry*-expressing animals were taken on a
602 Nikon NTi with a Nikon DS-Ri2 color camera with Nikon Elements software. Large full-
603 length images are comprised of several images stitched together. Confocal images were
604 captured using a Zeiss LSM 880 with LSM software and processed using Imaris 8.4.1
605 software (Bitplane LLC) to create 3D images from serial optical sections (z-stacks).
606 Images were then cropped and assembled using Photoshop and Illustrator (Adobe).
607 Live video was captured on a Nikon Eclipse E1000 microscope with Nikon
608 Imaging software. Movies were processed with ImageJ/Fiji software and screen shots
609 were obtained from individual frames, then cropped and assembled using Adobe
610 Photoshop and Illustrator.
611
612 **Statistical analysis**
613 For the regeneration and feed/starve experiments, mixed analysis of variance
614 (ANOVA) tests were used to analyze each dependent variable (i.e. the number of
615 longitudinal and tripolar neurons quantified). For both experiments, each observation of
616 an individual over time served as the within-subject factor (Regeneration experiment:
617 time 0 cut, 24hpa, 7dpa; Feed/starve: week 1, week of feeding regime switch, week 14).
618 The between subject factors used were animal size category (small: 20-40mm, medium:
619 41-60mm, medium-large: 61-80mm, large: 81-100mm) and assigned feeding group

(Feed-Starve or Starve-Feed) for the regeneration and feed/starve experiments respectively. A mixed ANOVA was also used to analyze changes in oral-aboral length during the feed/starve experiment, with each observation of an individual serving as the within-subject factor (week 1, week of feeding regime switch, and week 14) and assigned feeding group as the between-subject factor (Feed-Starve or Starve-Feed). Data used for ANOVA tests met assumptions of normality and homogeneity. Greenhouse-Geisser corrected F-statistics were reported if sphericity was violated (i.e. Figure 1I). When omnibus ANOVA results were significant, post-hoc testing was performed using Bonferroni corrections in order to maintain tight control over the type 1 error rate. Effect sizes are reported as partial eta^2 (η_p^2). Full AVONA model results are reported in Supplemental Document 1. Paired t-tests were used to compare individual changes in the number of neurons or length at two time points. All data were analyzed using SPSS version 21.0.

Acknowledgements

We would like to thank David Balli and Omar Ahmed for providing help with R software and construction of the line graphs. We also thank Dylan Faltine-Gonzalez, Noor Baban, and Brianna Maslonka for their help with maintenance of the animal stocks. This work was funded by the National Institutes of Health Award Number R01GM127615.

Competing Interests Statement

The authors declare that they have no financial or non-financial competing interests

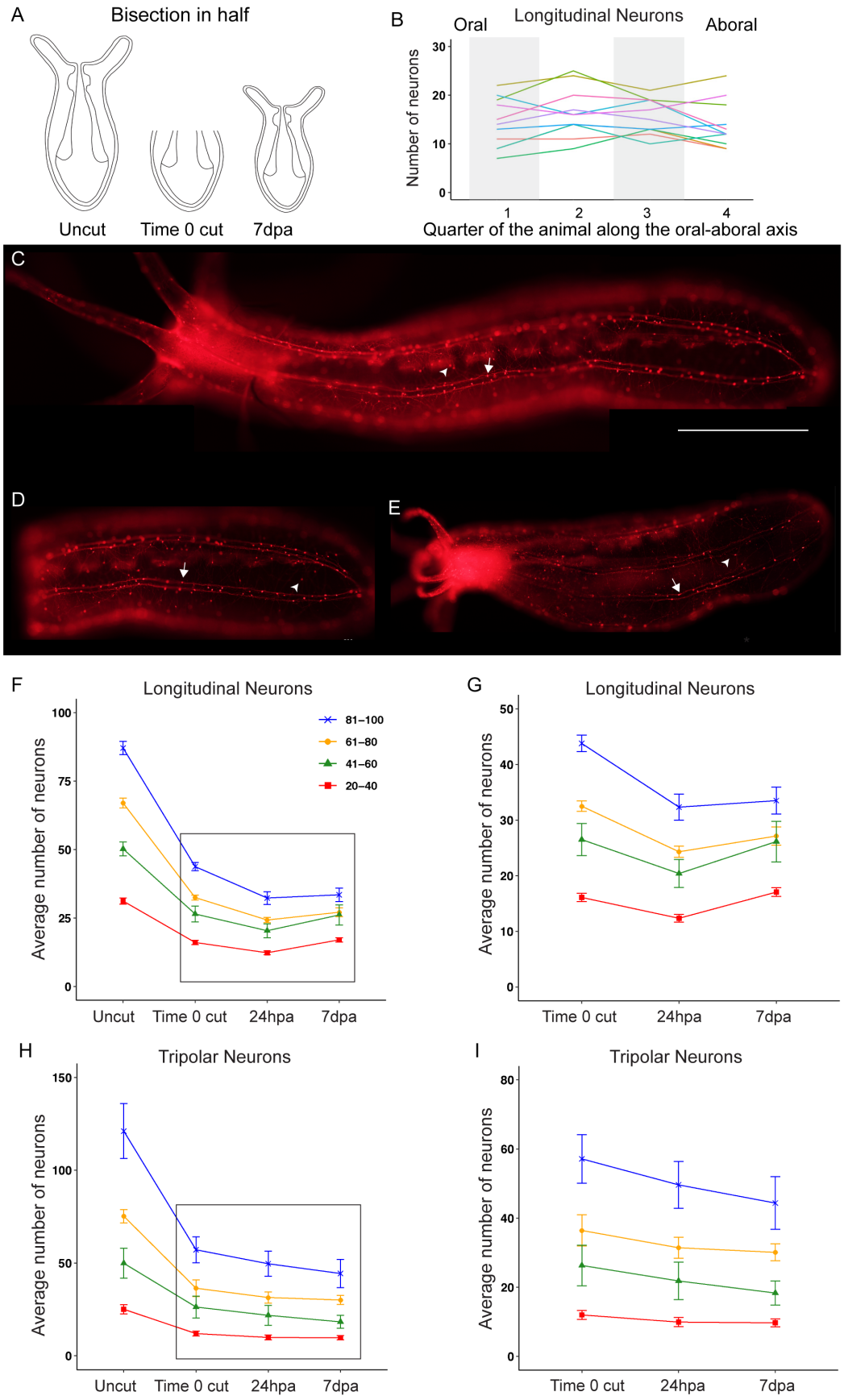
A
Bisection in half
Uncut
Time 0 cut
7dpa
B
Oral
Longitudinal Neurons
Aboral
Number of neurons
Quarter of the animal along the oral-aboral axis
C
D
E
F
Longitudinal Neurons
Average number of neurons
81–100
61–80
41–60
20–40
Uncut
Time 0 cut
24hpa
7dpa
G
Longitudinal Neurons
Average number of neurons
Time 0 cut
24hpa
7dpa
H
Tripolar Neurons
Average number of neurons
Uncut
Time 0 cut
24hpa
7dpa
I
Tripolar Neurons
Average number of neurons
Time 0 cut
24hpa
7dpa

651

Figure 1: Differential regeneration of *NvLWamide-like* neurons depends on the specific neuronal subtype. (A) Schematic for oral bisection at ~50% body length. (B) Quantification of the number of longitudinal neurons along the oral-aboral axis in each of the 4 equal quarters. Each line represents an individual animal. (C) Uncut *NvLWamide-like::mCherry* expressing animal. (D) Same animal as C at time 0 cut. (D) Same animal as C and D at 7 days post amputation (dpa), with regenerated oral structures. (F-I**)** Quantification of longitudinal and tripolar neurons before amputation (uncut), immediately following bisection at the O-A midline (time 0 cut), 24hpa, and at completion of regeneration (7dpa) in small (red), medium (green), medium-large (orange), and large (blue) sized animals. The numbers of longitudinal neurons (F) or tripolar neurons (H) never regenerate back to their original pre-cut numbers. (G) Longitudinal neurons regenerate back to numbers similar to time 0 cut in the small and medium sized animals, but do not regenerate in the larger animals by 7dpa. (I) Tripolar neurons do not regenerate by 7dpa. N = 40 animals. Scale bar = 1mm. ((G) Mixed ANOVA: interaction effect between animal size and observation time: $F_{6,70} = 10.27$, $p < 0.001$, $\eta_p^2 = 0.47$; (I) Mixed ANOVA: main effect of observation time Tripolar: $F_{1.4,46.9} = 20.70$, $p = < 0.001$, $\eta_p^2 = 0.38$). Data points in F-I represent mean ± SEM.

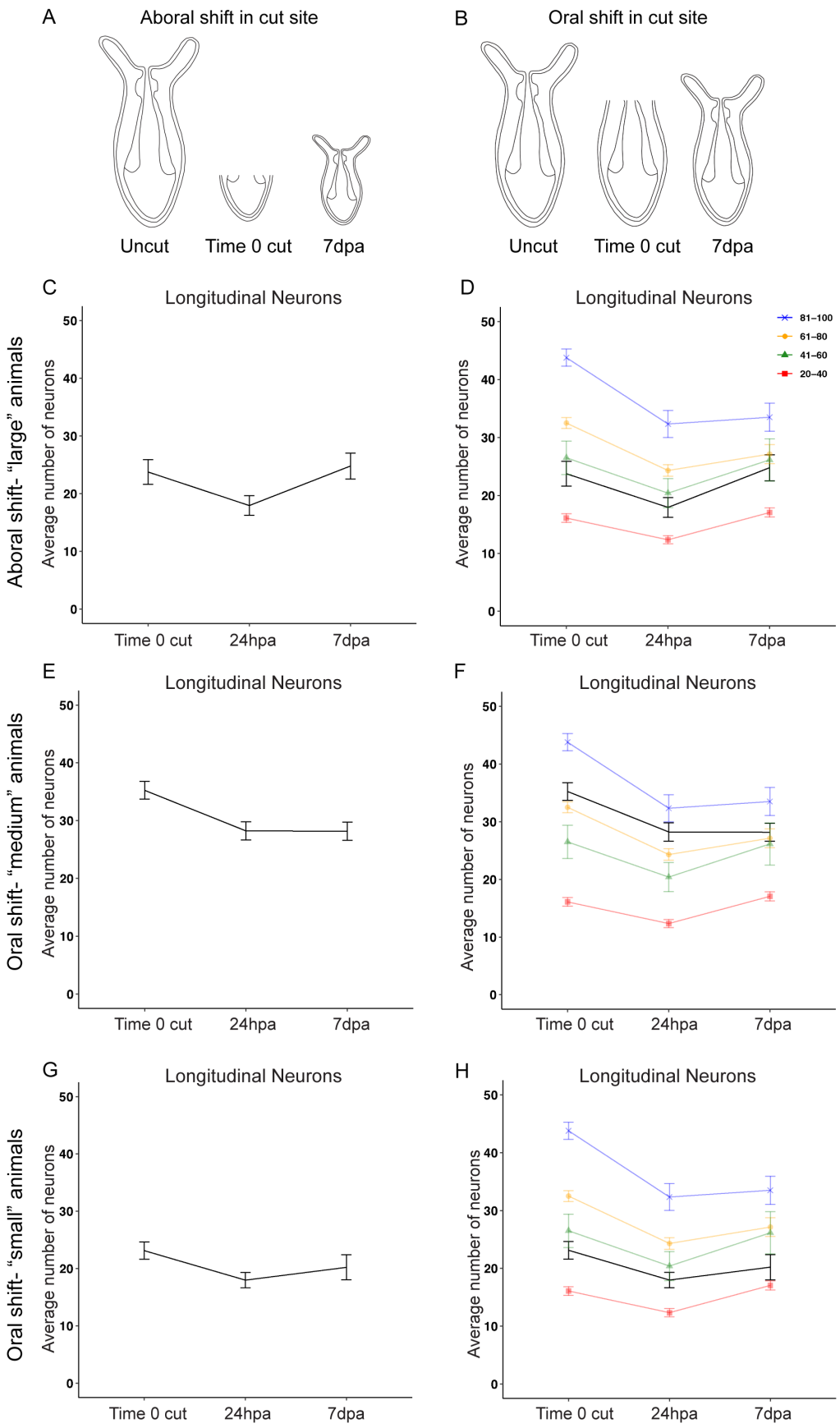
A
Aboral shift in cut site
Uncut
Time 0 cut
7dpa
B
Oral shift in cut site
Uncut
Time 0 cut
7dpa
C
Longitudinal Neurons
Aboral shift- "large" animals
Average number of neurons
Time 0 cut
24hpa
7dpa
D
Longitudinal Neurons
81–100
61–80
41–60
20–40
Average number of neurons
Time 0 cut
24hpa
7dpa
E
Longitudinal Neurons
Oral shift- "medium" animals
Average number of neurons
Time 0 cut
24hpa
7dpa
F
Longitudinal Neurons
Average number of neurons
Time 0 cut
24hpa
7dpa
G
Longitudinal Neurons
Oral shift- "small" animals
Average number of neurons
Time 0 cut
24hpa
7dpa
H
Longitudinal Neurons
Average number of neurons
Time 0 cut
24hpa
7dpa

683

Figure 2: Regeneration of longitudinal neurons depends on the size of the regenerating fragment. (A-B) Schematics demonstrating the shifts in cut sites used to obtain remnant fragments of varying sizes. (C-H) Quantification of longitudinal neurons in regenerates with shifted cut sites at time 0 cut, 24hpa, and 7dpa. Regenerates from an aborally-shifted cut site in large animals regenerated their longitudinal neurons (C), resembling regenerates of small and medium sized animals cut at the midline of the O-A axis (D). Regenerates from an orally-shifted cut site in medium animals did not regenerate their longitudinal neurons (E), resembling regenerates from large animals cut at the midline of the O-A axis (F). Regenerates from an orally-shifted cut site in small animals still regenerated their longitudinal neurons (G), resembling regenerates from medium animals cut at the midline of the O-A axis (H). N = 8 large; 13 medium; 13 small. Arrows indicate longitudinal neurons and arrowheads indicate tripolar neurons (Repeated measure ANOVA comparing observation times: (C) Large, $F_{2,14} = 5.58$, $p = 0.017$, $\eta_p^2 = 0.44$; (E) Medium, $F_{2,24} = 21.67$, $p < 0.001$, $\eta_p^2 = 0.64$; (G) Small, $F_{2,24} = 8.56$, $p = 0.002$, $\eta_p^2 = 0.42$). Data points in C-H represent mean ± SEM.

715

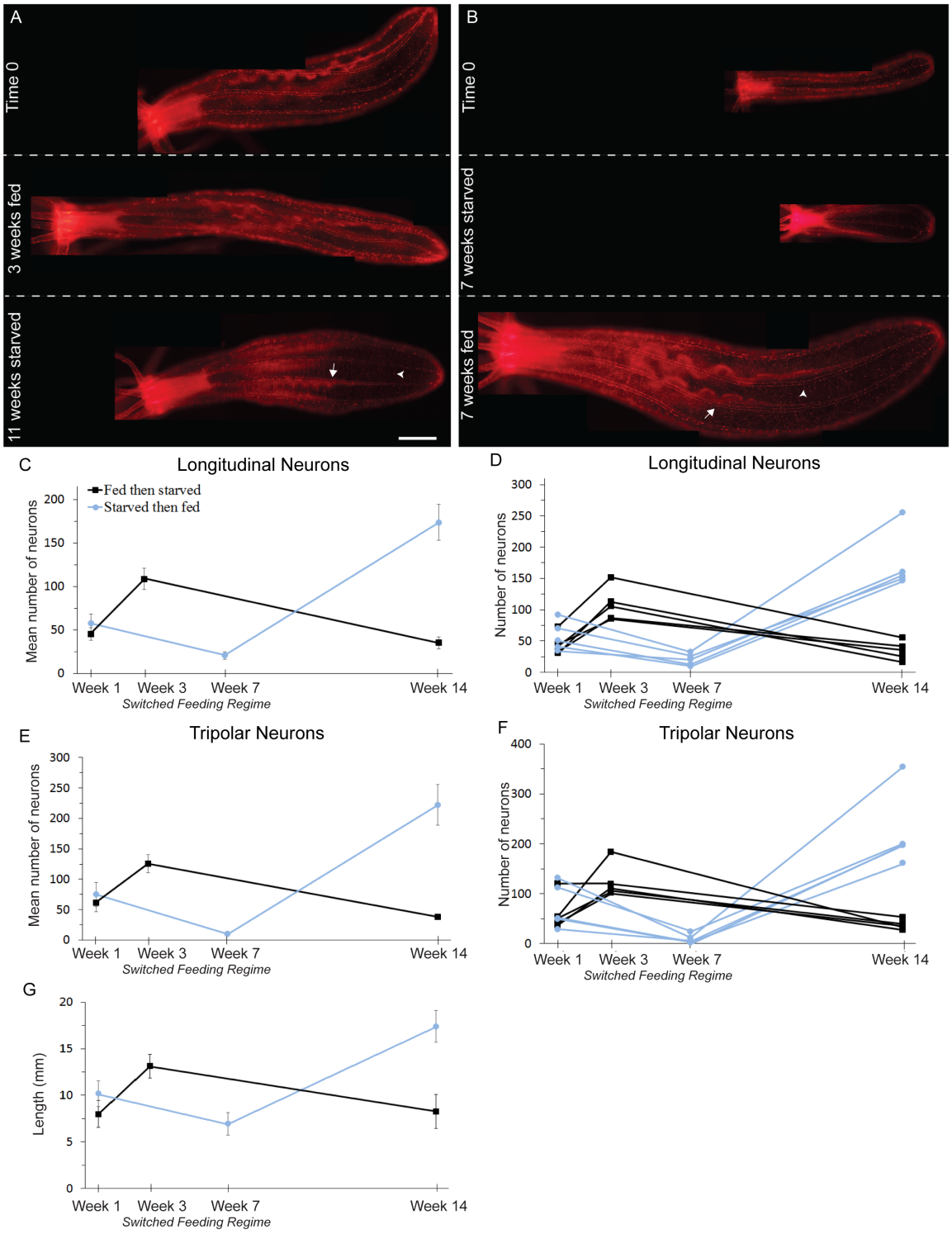

716

717 **Figure 3: The *Nematostella* nerve net scales with changes in length.** (A-B)
718 Visualization of *NvLWamide-like* neurons in relation to body size during periods of
719 feeding and starvation. (C-F) Quantification of *NvLWamide-like* neurons during periods

of growth and starvation with both mean (C, E) and population (D, F) data presented. Animals fed for 3 weeks rapidly grew longer in length (A, 3 weeks fed), and numbers of both longitudinal (C and D, black lines) and tripolar (E and F, black lines) neurons significantly increased. Following 11 weeks starvation, the same animal then shrunk in size (A, 11 weeks starved) and the numbers of both longitudinal and tripolar neurons significantly decreased (C-F, black lines). Animals initially starved for 7 weeks shrunk in size (B, 7 weeks starved) and number of both longitudinal (C and D, blue lines) and tripolar (E and F, blue lines) significantly decreased. Upon being switched to feeding regime for 7 weeks the same animals grew longer (B, 7 weeks starved) and the numbers of both longitudinal and tripolar neurons significantly increased (C-F, blue lines). Oral end is to the left. Scale bar = 1mm. N = 5 animals per treatment group. Arrows indicate longitudinal neurons and arrowheads indicate tripolar neurons. (Mixed ANOVA of interaction between assigned feeding regime and observation time: (C) Longitudinal, $F_{2,16} = 102.01$, $p < 0.001$, $\eta_p^2 = 0.93$; (E) Tripolar, $F_{2,16} = 48.60$, $p < 0.001$, $\eta_p^2 = 0.86$). (G) The measured length of the animals significantly decreased during the starvation period and increased during the feeding period (Mixed ANOVA: interaction effect between assigned feeding regime and observation time: $F_{2,34} = 25.75$, $p < 0.001$, $\eta_p^2 = 0.60$). Data points in C, E and G represent mean ± SEM.

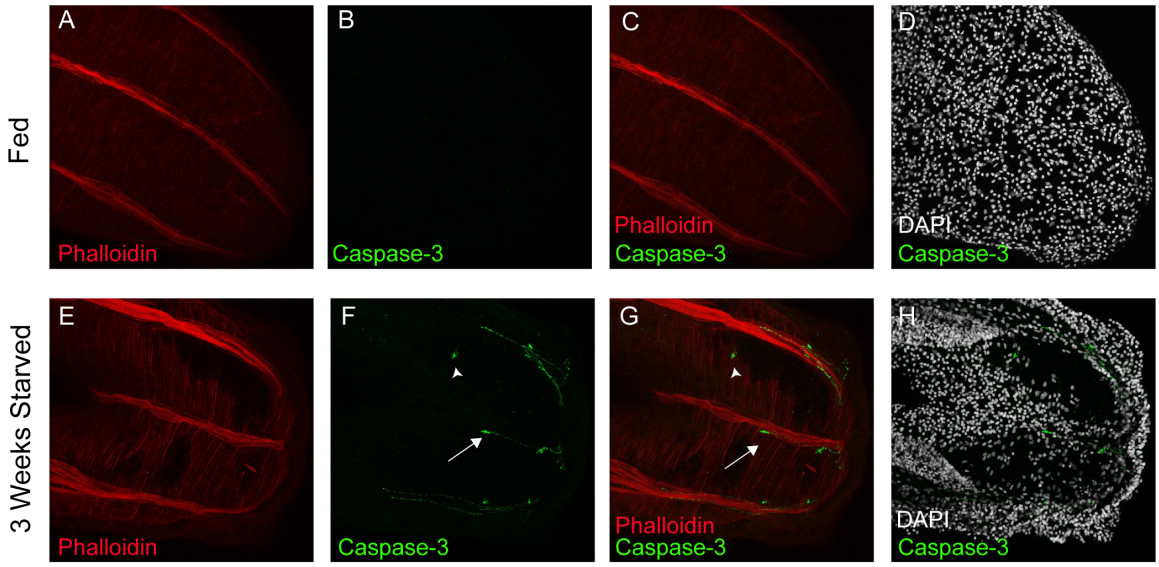

Figure 4: Increased apoptosis in 3-week starved animals. (A-D) Normally fed animals did not have activated Caspase-3 staining in the most aboral region in 14 out of 16 animals examined (2/16 had positive staining, data not shown). (E-H) Animals that were starved for 3 weeks had positive Caspase-3 visible in the most aboral region in 15 out of 15 animals examined. (F-H) Caspase-3 was located along the endodermal longitudinal tracks in the most aboral region (arrow) and in the aboral body column (arrowhead).

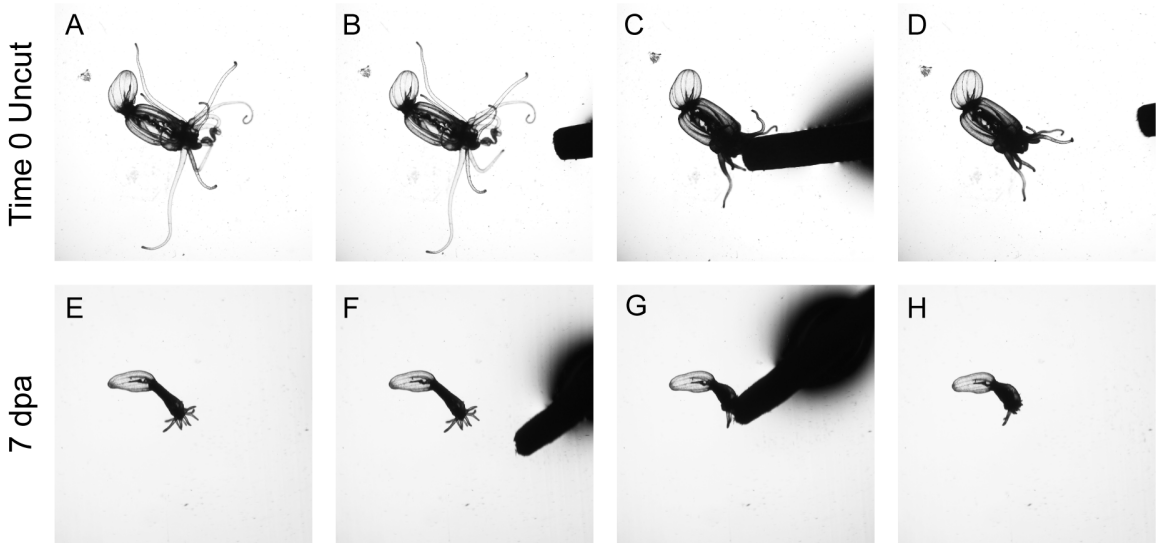

Figure 5: Response to poking assay is maintained in regenerating animals. (A-D) *Nematostella* respond to the touch stimulus by retracting its tentacles when touched with a toothpick (N = 8/8). (E-H) At 7 days post amputation the same animal again responded to being poked with a toothpick by retracting its tentacles (N = 8/8).

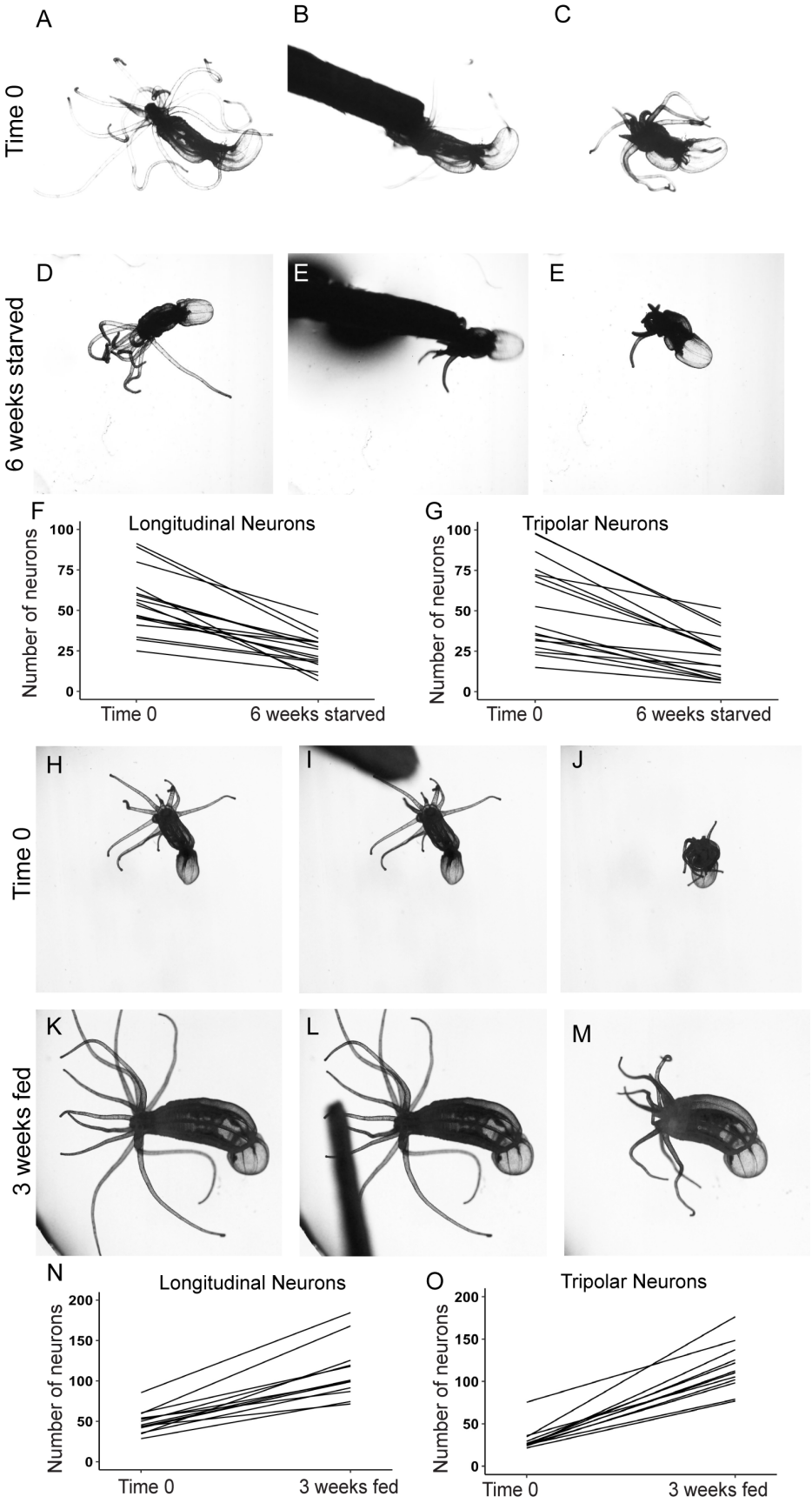
A
B
C
Time 0
D
E
E
6 weeks starved
F
Longitudinal Neurons
Number of neurons
100
75
50
25
0
Time 0
6 weeks starved
G
Tripolar Neurons
Number of neurons
100
75
50
25
0
Time 0
6 weeks starved
H
I
J
Time 0
K
L
M
3 weeks fed
N
Longitudinal Neurons
Number of neurons
200
150
100
50
0
Time 0
3 weeks fed
O
Tripolar Neurons
Number of neurons
200
150
100
50
0
Time 0
3 weeks fed

795

Figure 6: Starved and fed animals respond to the Poking assay by retracting their tentacles and body. (A-E) A normally fed animal responded to the touch stimulus from a toothpick by retracting its tentacles and oral region (N = 17/19). (D-E) Following 6-7 weeks starvation, the same animal again responded to being touched with a toothpick by retracting its tentacles and oral region (N = 17/19). (F-G) Quantification of the number of longitudinal and tripolar neurons in individual animals following each poking experiment. The numbers of both longitudinal (I: $t_{16} = 7.97$, $p < 0.001$, $\eta_p^2 = 0.80$) and tripolar (J: $t_{16} = 6.99$, $p < 0.001$, $\eta_p^2 = 0.75$) neurons significantly decreased after 6-7 weeks starvation. (H-J) A normally fed animal responded to the touch stimulus from a toothpick by retracting its tentacles and body (N = 13/13). (K-M) Following 3 weeks feeding, the same animal again responded to being touched with a toothpick by retracting its tentacles and oral region (N = 12/13). (N-O) Quantification of the number of longitudinal and tripolar neurons in individual animals following each poking experiment. The numbers of both longitudinal (G: $t_{12} = -9.15$, $p < 0.001$, $\eta_p^2 = 0.88$) and tripolar (H: p = $t_{12} = -12.76$, $p < 0.001$, $\eta_p^2 = 0.93$) neurons significantly increased following 3 weeks feeding.

826 **Table 1:** Summary of the analysis for the action-reaction Poking assay in regenerated,
827 starved, and fed animals.
828

Treatment	Timepoint	Number of animals that responded to the touch stimulus	Percent of animals that responded to the touch stimulus
Regeneration	Uncut	8/8	100%
	7dpa	8/8	100%
Starved	Time 0	17/19	89%
	6-7 weeks starved	17/19	89%
Fed	Time 0	13/13	100%
	3 weeks fed	12/13	92%

829
830
831
832
833
834
835
836
837
838
839
840
841
842
843
844
845
846
847
848
849
850

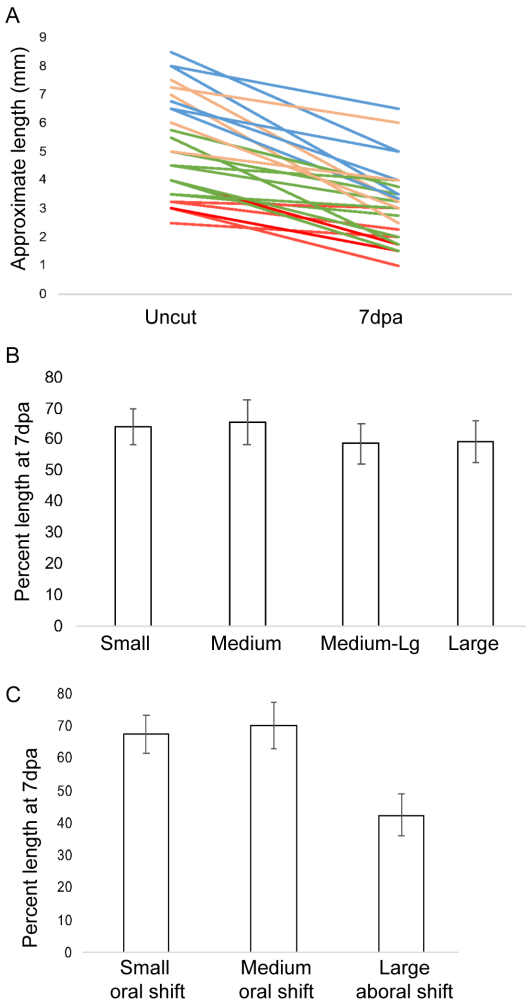

Supplemental Figure 1: Regenerated *Nematostella* did not return to their original length by 7dpa. Length was measured with a ruler under a dissection microscope at the start of the experiment before oral bisection ("Uncut"). The animals never re-grew back to their original length, and there was no difference in the percent length of the regenerates relative to their body size by 7dpa. (A) Percent length for animals bisected in half. N = 11 small; 8 medium; 6 medium-large; 6 large (One way ANOVA: $F_{3,27} = 0.23$, $p = 0.875$, $\eta_p^2 = 0.025$). (B) Population data showing lengths for individual animals before they were cut (uncut) and 7dpa. Small animals are represented in red, medium in green, medium-large in orange, and large in blue ($t_{30} = 8.65$, $p < 0.001$, $\eta_p^2 = 0.71$). N = 31 animals. (C) Percent length for animals with the shifted cut sites. N = 13 small oral shift; 11 medium oral shift; 7 large aboral shift (One way ANOVA: $F_{2,17} = 8.12$, $p = 0.003$, $\eta_p^2 = 0.488$). Bars in A and C represent mean ± SEM.

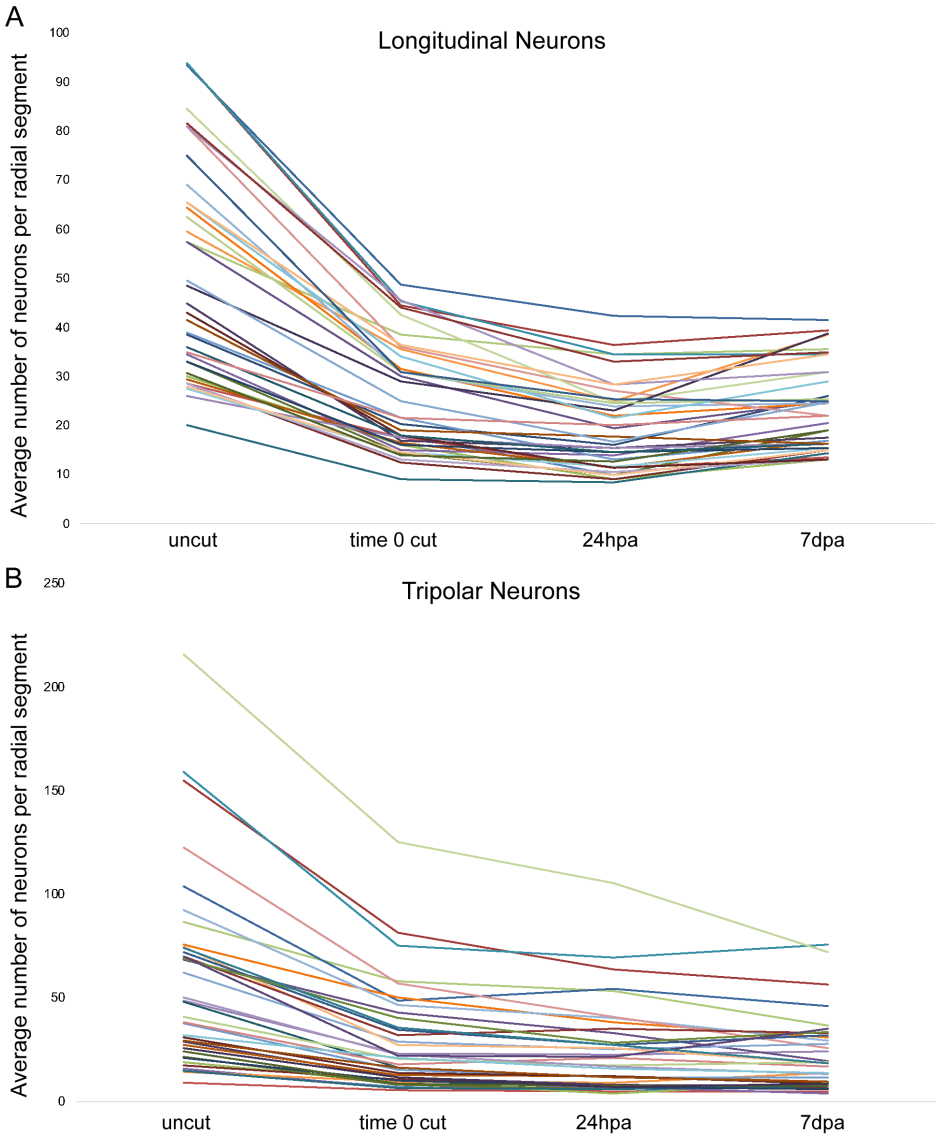

Supplemental Figure 2: Quantification of neuronal numbers during oral regeneration per individual regenerating animal. Population data showing the time course of the average number of (A) longitudinal neurons and (B) tripolar neurons per 2-3 radial segments in individual regenerating animals bisected in half. Neuronal numbers do not return to levels present in the uncut animal. Quantifications were taken before cutting (uncut), time 0 cut, 24hpa, and 7dpa. N = 40 animals. Data represented here is the same dataset grouped by starting size and averaged in Figure 1.

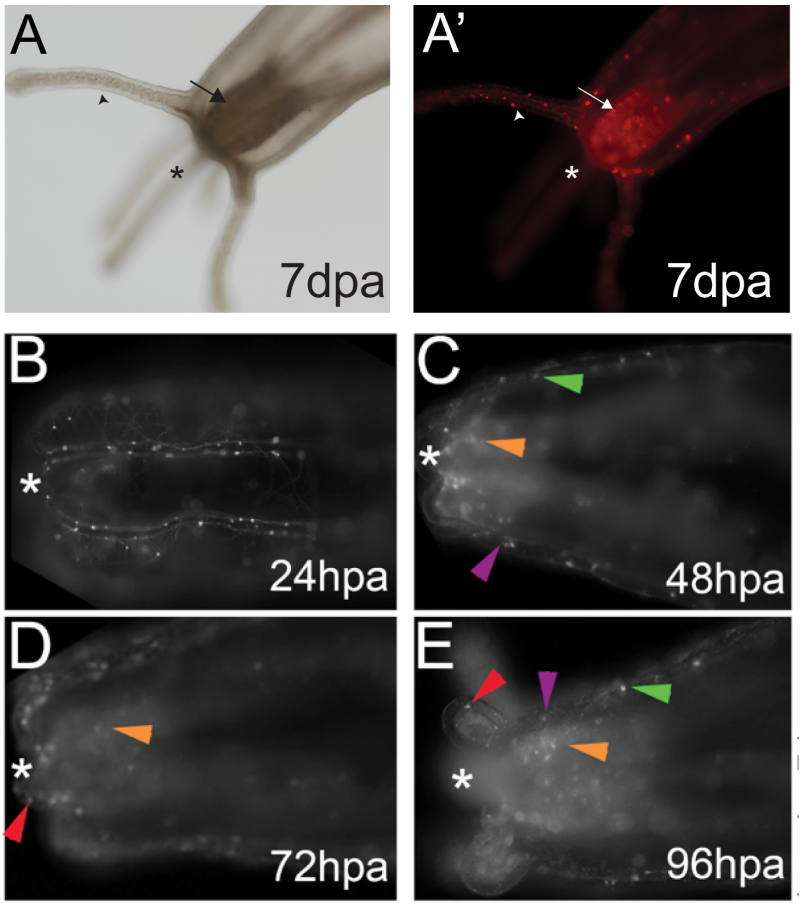

Supplemental Figure 3. Regeneration of oral structures and neurons in *NvLWamide-like::mCherry* animals following bisection along the O-A axis. (A) Regenerated oral structures, including a mouth, pharynx (arrow), and tentacles at 7dpa. (A') New neurons are observed in the regenerated oral structures, including pharyngeal (arrow) and tentacular (arrowhead) neurons. (B) Remnant fragment at 24hpa. No new structures are observed at this timepoint. (C) Tentacle buds are visible in the remnant fragment at 48hpa. Longitudinal (green arrowhead) and tripolar (purple arrowhead) neurons are observed. Regenerated pharyngeal neurons are also present in the regenerating pharynx (orange arrowhead) at 48hpa. (D) Pharyngeal (orange arrowhead) and tentacular (red arrowhead) neurons are clearly visible in these regenerating structures by 72hpa. (E) Clearly regenerated pharyngeal (orange arrowhead) and tentacular (red arrowhead) neurons are seen at 96hpa. Longitudinal neurons (green arrowhead) also populate the regenerated tissue, but if these are regenerated neurons or from the remnant is undetermined. Asterisks indicate oral opening.

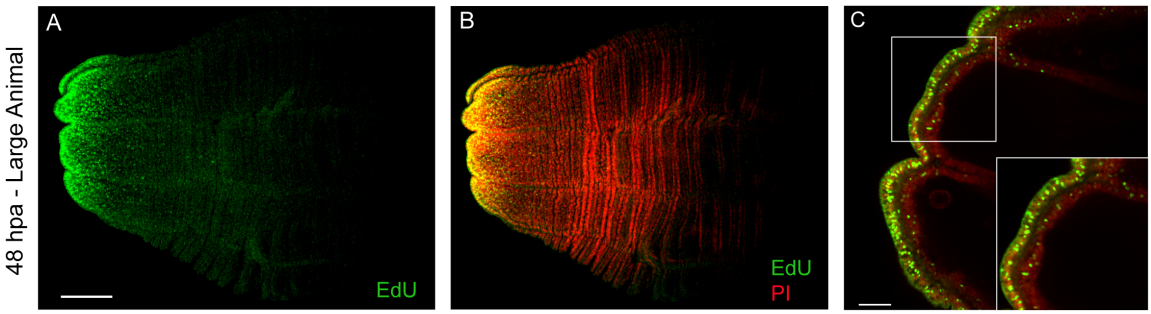

Supplemental Figure 4: Detection of proliferating cells in "large" *Nematostella* during oral regeneration. (A) EdU (green) is detected at 48hpa in the oral-most region of "large" regenerating animals bisected in half. (B) EdU overlaid with propidium iodide (PI, red) stain in the same animal as A, with yellow color showing co-expression. (C) Higher magnification image of the same animal, showing EdU detection in both the ectoderm and endoderm, suggesting both tissue layers proliferate during oral regeneration. N = 3 large animals. Scale bars for A and B = 200um; C = 50um.

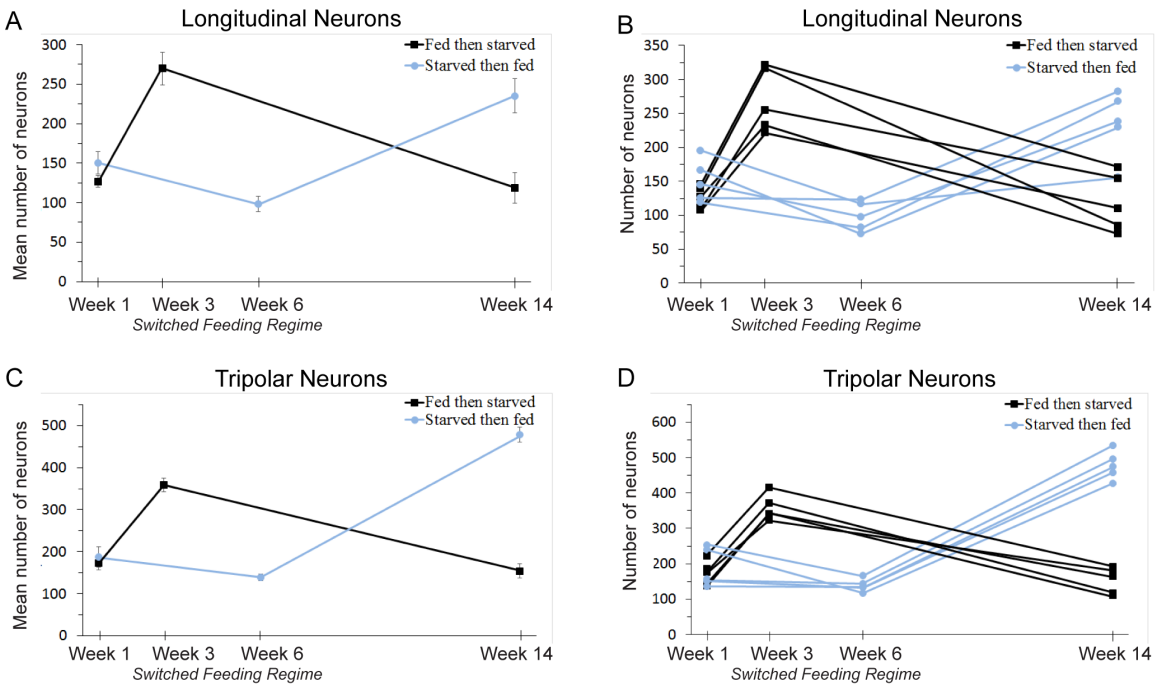

Supplemental Figure 5: Independent experiment demonstrating *Nematostella* nerve net scales with changes in length. (A-D) Quantification of *NvLWamide-like* neurons during periods of feeding and starvation with both mean (A,C) and population (B,D) data presented. The numbers of both longitudinal (A and B, black lines) and tripolar (C and D, black lines) neurons significantly increased with 3 weeks of feeding, and then both longitudinal and tripolar neurons significantly decreased with 11 weeks starvation (A-D, black lines). The numbers of both longitudinal (A and B, blue lines) and tripolar (C and D, blue lines) significantly decreased following 6 weeks starvation. Upon being switched to feeding regime for 8 weeks the numbers of both longitudinal and tripolar neurons significantly increased (A-D, blue lines) (Mixed ANOVA: interaction effect between assigned feeding regime and observation time: (A) Longitudinal, $F_{2,16} = 38.88$, $p < 0.001$, $\eta_p^2 = 0.83$; (C) Tripolar, $F_{2,16} = 206.13$, $p < 0.001$, $\eta_p^2 = 0.96$). Data points in A and C represent mean ± SEM.

938 **References**
939

940 Amiel, A.R. et al., 2015. Characterization of Morphological and Cellular Events
941 Underlying Oral Regeneration in the Sea Anemone, Nematostella vectensis.
942 *International Journal of Molecular Sciences*, 16(12), pp.28449–28471.

943 Baguna, J., Romero, R.Romero, 1981. Quantitative anlaysis of cell types during growth,
944 degrowth, and regeneration in the planarians Dugesia mediterranea and Dugesia
945 tigrina. *Hydrobiologia*, 84, pp.181–194.

946 Bossert, P.E., Dunn, M.P. & Thomsen, G.H., 2013. A staging system for the regeneration
947 of a polyp from the aboral physa of the anthozoan Cnidarian Nematostella vectensis.
948 *Developmental Dynamics*, 242(11), pp.1320–1331.

949 Bowers, M. et al., 2015. BLOOD582924 2678..2688. *Blood*, 125(17), pp.2678–2688.

950 Busengdal, H. & Rentzsch, F., 2017. Unipotent progenitors contribute to the generation
951 of sensory cell types in the nervous system of the cnidarian Nematostella vectensis.
952 *Developmental biology*, 431(1), pp.59–68.

953 Caldwell, L.J. et al., 2019. Regeneration of Dopaminergic Neurons in Adult Zebrafish
954 Depends on Immune System Activation and Differs for Distinct Populations. *The*
955 *Journal of Neuroscience*, 39(24), pp.4694–4713.

956 Calvi, L.M. et al., 2003. Identification of the haematopoietic stem cell niche and control
957 of the niche size. *Nature*, 425(6960), pp.841–846.

958 Cebrià, F. et al., 2002. Dissecting planarian central nervous system regeneration by the
959 expression of neural-specific genes. *Development, Growth & Differentiation*, 44(2),
960 pp.135–146.

961 Chen, C.C.G., Wang, I.E. & Reddien, P.W., 2013. pbx is required for pole and eye
962 regeneration in planarians. 140(4), pp.719–729.

963 Currie, K.W. & Pearson, B.J., 2013. Transcription factors lhx1/5-1 and pitx are required
964 for the maintenance and regeneration of serotonergic neurons in planarians.
965 *Development*, 140(17), pp.3577–3588.

966 Deochand, M.E., Birkholz, T.R. & Beane, W.S., 2016. Temporal regulation of planarian
967 eye regeneration. *Regeneration*, 3(4), pp.209–221.

968 D'Amelio, M., Sheng, M. & Cecconi, F., 2012. Caspase-3 in the central nervous system:
969 beyond apoptosis. *Trends in Neurosciences*, 35(11), pp.700–709.

970 Elmore, S., 2016. Apoptosis: A Review of Programmed Cell Death. *Toxicologic*
971 *Pathology*, 35(4), pp.495–516.

972 Fritz, A.E. et al., 2013. Mechanisms of tentacle morphogenesis in the sea anemone

973 Nematostella vectensis. *Development*, 140(10), pp.2212–2223.

974 Gahan, J.M. et al., 2017. Functional studies on the role of Notch signaling in Hydractinia
975 development. *Developmental biology*, 428(1), pp.224–231.

976 Galliot, B. et al., 2007. RNAi gene silencing affects cell and developmental plasticity in
977 hydra. *Comptes Rendus Biologies*, 330(6-7), pp.491–497.

978 Hand, C. & Uhlinger, K.R., 1992. The Culture, Sexual and Asexual Reproduction, and
979 Growth of the Sea Anemone *Nematostella vectensis*. *Biological Bulletin*, 182,
980 pp.169–176.

981 Havrilak, J.A. et al., 2017. Characterization of NvLWamide-like neurons reveals
982 stereotypy in Nematostella nerve net development. *Developmental biology*, pp.1–0.

983 Jahnel, S.M., Walzl, M. & Technau, U., 2014. Development and epithelial organisation
984 of muscle cells in the sea anemone Nematostella vectensis. 11(1), pp.1–15.

985 Kuida, K. et al., 1996. Decreased apoptosis in the brain and premature lethality in
986 CPP32-deficient mice. *Nature*, 384, pp.368–372.

987 Layden, M.J. et al., 2010. Expression and phylogenetic analysis of the zic gene family in
988 the evolution and development of metazoans. *EvoDevo*, 1(1), p.12. Available at:
989 http://eutils.ncbi.nlm.nih.gov/entrez/eutils/elink.fcgi?dbfrom=pubmed&id=21054859
990 &retmode=ref&cmd=prlinks.

991 Layden, M.J. et al., 2016. MAPK signaling is necessary for neurogenesis in Nematostella
992 vectensis. *BMC Biology*, 14(1), p.61.

993 Leclère, L. et al., 2016. Development of the aboral domain in Nematostella requires β-
994 catenin and the opposing activities of Six3/6 and Frizzled5/8. *Development*, 143(10),
995 pp.1766–1777.

996 Marlow, H., Matus, D.Q. & Martindale, M.Q., 2013. Ectopic activation of the canonical
997 wnt signaling pathway affects ectodermal patterning along the primary axis during
998 larval development in the anthozoan Nematostella vectensis. *Developmental biology*,
999 380(2), pp.324–334.

1000 Miljkovic-Licina, M. et al., 2007. Head regeneration in wild-type hydra requires de novo
1001 neurogenesis. 134(6), pp.1191–1201.

1002 Moya, A. et al., 2016. Functional conservation of the apoptotic machinery from coral to
1003 man: the diverse and complex Bcl-2 and caspase repertoires of Acropora millepora.
1004 *BMC Genomics*, pp.1–21.

1005 Nakanishi, N. et al., 2012. Nervous systems of the sea anemone Nematostella vectensis
1006 are generated by ectoderm and endoderm and shaped by distinct mechanisms.
1007 *Development*, 139(2), pp.347–357.

1008 Oviedo, N.J., Newmark, P.A. & Sánchez Alvarado, A., 2003. Allometric scaling and
1009 proportion regulation in the freshwater planarian Schmidtea mediterranea.
1010 *Developmental Dynamics*, 226(2), pp.326–333.

1011 Passamaneck, Y.J. & Martindale, M.Q., 2012. Cell proliferation is necessary for the
1012 regeneration of oral structures in the anthozoan cnidarian Nematostella vectensis.
1013 *BMC Developmental Biology*, 12(1), p.34.

1014 Renfer, E. et al., 2010. A muscle-specific transgenic reporter line of the sea anemone,
1015 Nematostella vectensis. *Proceedings of the National Academy of Sciences of the*
1016 *United States of America*, 107(1), pp.104–108.

1017 Rentzsch, F., Layden, M. & Manuel, M., 2016. The cellular and molecular basis of
1018 cnidarian neurogenesis. *Wiley Interdisciplinary Reviews: Developmental Biology*,
1019 pp.1–19.

1020 Richards, G.S. & Rentzsch, F., 2014. Transgenic analysis of a SoxB gene reveals neural
1021 progenitor cells in the cnidarian Nematostella vectensis. *Development*, 141(24),
1022 pp.4681–4689.

1023 Roberts-Galbraith, R.H., Brubacher, J.L. & Newmark, P.A., 2016. A functional genomics
1024 screen in planarians reveals regulators of whole-brain regeneration. *eLIFE*, pp.1–31.

1025 Romero, R. & BAGUÑÀ, J., 1991. Quantitative cellular analysis of growth and
1026 reproduction in freshwater planarians (Turbellaria; Tricladida). I. A cellular
1027 description of the intact organism. *Invertebrate Reproduction & Development*, 19(2),
1028 pp.157–165.

1029 Röttinger, E., Dahlin, P. & Martindale, M.Q., 2012. A Framework for the Establishment
1030 of a Cnidarian Gene Regulatory Network for "Endomesoderm" Specification: The
1031 Inputs of ß-Catenin/TCF Signaling M. C. Mullins, ed. *PLoS Genetics*, 8(12),
1032 p.e1003164.

1033 Siebert, S. et al., 2018. Stem cell differentiation trajectories in Hydra resolved at single-
1034 cell resolution. pp.1–29.

1035 Sinigaglia, C. et al., 2013. The bilaterian head patterning gene six3/6 controls aboral
1036 domain development in a cnidarian. *PLoS Biology*, 11(2), p.e1001488.

1037 Steinmetz, P.R.H. et al., 2017. Gut-like ectodermal tissue in a sea anemone challenges
1038 germ layer homology. *Nature Ecology & Evolution*, 1(10), pp.1–0.

1039 Takeda, H., Nishimura, K. & Agata, K., 2009. Planarians Maintain a Constant Ratio of
1040 Different Cell Types During Changes in Body Size by Using the Stem Cell System.
1041 *Zoological Science*, 26(12), pp.805–813.

1042 Tay, T.L. et al., 2017. A new fate mapping system reveals context-dependent random or
1043 clonal expansion of microglia. *Nature Neuroscience*, 20(6), pp.793–803.

1044 Tucker, R.P., Shibata, B. & Blankenship, T.N., 2011. Ultrastructure of the mesoglea of
1045 the sea anemone Nematostella vectensis (Edwardsiidae). *Invertebrate Biology*,
1046 130(1), pp.11–24.

1047 van Ham, T.J. et al., 2014. Intravital correlated microscopy reveals differential
1048 macrophage and microglial dynamics during resolution of neuroinflammation.
1049 *Disease Models & Mechanisms*, 7(7), pp.857–869.

1050 Warner, J.F. et al., 2019. Regeneration is a partial redeployment of the embryonic gene
1051 network. *bioRxiv*, 121, pp.1731–28.

1052 Williams, R.B., 1975. A redescription of the brackish-water sea anemone *Nematostella*
1053 *vectensis* Stephenson, with an appraisal of congeneric species. *Journal of Natural*
1054 *History*, 9(1), pp.51–64.

1055 Zhang, J. et al., 2003. Identification of the haematopoietic stem cell niche and control of
1056 the niche size. *Nature*, 425(6960), pp.836–841.

1057